Natural Convection in a Saturated Variable-Porosity Medium Due to Microwave Heating

Watit Pakdee[1]
e-mail: pwatit@engr.tu.ac.th
e-mail: wpele95@yahoo.com

Phadungsak Rattanadecho

Department of Mechanical Engineering,
Research Center of Microwave Utilization in Engineering (RCME),
Thammasat University,
Klong Luang,
Pathumthani, Thailand

Microwave heating of a porous medium with a nonuniform porosity is numerically investigated based on a proposed numerical model. A two-dimensional variation of porosity of the medium is considered. The generalized non-Darcian model developed takes into account the presence of a solid drag and the inertial effect. The transient Maxwell's equations are solved by using the finite difference time domain method to describe the electromagnetic field in the waveguide and medium. The temperature profile and velocity field within a medium are determined by solution of the momentum, energy, and Maxwell's equations. The coupled nonlinear set of these equations is solved using the SIMPLE algorithm. In this work, a detailed parametric study is conducted on heat transport inside a rectangular enclosure filled with a saturated porous medium of constant or variable porosity. The numerical results agree well with the experimental data. Variations in porosity significantly affect the microwave heating process as well as the convective flow pattern driven by microwave energy. [DOI: 10.1115/1.4003535]

Keywords: microwave heating, variable porosity, natural convection, saturated porous media, rectangular waveguide

1 Introduction

Microwave heating of a porous medium is widely implemented in industries, such as heating food, ceramics, biomaterials, concrete manufacture, etc., since microwave energy has many advantages such as short time process, high thermal efficiency, environmentally friendly credentials, and high product quality. Microwave radiation penetrates into a material and heats it by a dipolar polarization that occurs million times per second.

A number of previous works have focused on the drying of unsaturated porous media in which heat and mass transfers were modeled [1–6]; however, most of these dealt with solid materials and focused on heat conduction within a medium. Some works studied a natural convection induced by microwave heating of fluids since a complex distribution of electromagnetic waves is shown to be a complicated effect on flow field [7–11]. The effects of natural convection and dielectric properties on liquid layers were studied numerically and experimentally. The heating kinetics strongly depended on the dielectric properties [7]. Natural convection due to buoyancy force strongly affects flow patterns within the water layer during the microwave heating process and clearly enhances temperature distribution in the layer [8]. Recently, Cha-um et al. [8] experimentally investigated the heating process within a packed bed filled with glass beads and water and found that the location of the sample relative to that of heat source had an important effect on the pattern of heating. Other recent works focused on microwave driven convection in pure liquids [9–11]. While the previous studies were based on pure liquids, we pay attention to a natural convection induced by microwave energy in a fluid-saturated porous medium.

Furthermore, all the previous investigations referred did not account for the effect of variable porosity in the vicinity of the impermeable wall. A region of higher porosity near the wall that forms due to the packing of the porous spheres near the column wall is not as efficient as that away from the wall toward the column center [12]. Benenati and Brosilow [13] found a distinct porosity variation with a high porosity region close to the wall in packed beds. Values of porosity that are highly close to an impermeable wall decrease to an asymptotic value at about four to five sphere diameters away from it [14,15]. Many researchers found that the variation of porosity might significantly affect flow patterns as well as heat transfer features [13,16–18]. The porosity of the bed exhibits sinusoidally damping decay especially at locations near the wall [13]. This phenomenon leads to the channeling effect that could significantly modify flow patterns [14,19–21]. Hsiao et al. [17] showed that including the effects of variable porosity and thermal dispersion on natural convection in the region of the heated horizontal cylinder in an enclosed porous medium increases the average Nusselt number and reduces the error between the experimental data and their solutions. Thus, the effects of porosity variation should be taken into account in practice [16,17,22,23].

Therefore, in the present study, we propose a numerical model for the microwave heating of a saturated porous packed bed in which the porosity variation is considered. The non-Darcian boundary and inertial effects are taken into account. Heating characteristic and flow pattern are numerically investigated. The numerical model is validated with experimental data obtained using a rectangular waveguide operated under the microwave of TE_{10} mode.

2 Experimental Setup

Figure 1 shows the experiment apparatus for microwave heating of a saturated porous medium using a rectangular waveguide. Actual image of the apparatus is shown in Fig. 1(*a*). The microwave system is a monochromatic wave of TE_{10} mode operating at a frequency of 2.45 GHz. From Fig. 1(*b*), magnetron (No. 1) generates microwaves and transmits them along the *z*-direction of the rectangular waveguide (No. 5) with inside cross-sectional dimension of 109.2×54.61 mm^2 that refers to a testing area (circled) and a water load (No. 8) that is situated at the end of the waveguide. On the upstream side of the sample, an isolator is used to trap any microwaves reflected from the sample to prevent dam-

[1]Corresponding author.

Contributed by the Heat Transfer Division of ASME for publication in the JOURNAL OF HEAT TRANSFER. Manuscript received May 11, 2010; final manuscript received January 14, 2011; published online March 8, 2011. Assoc. Editor: William P. Klinzing.

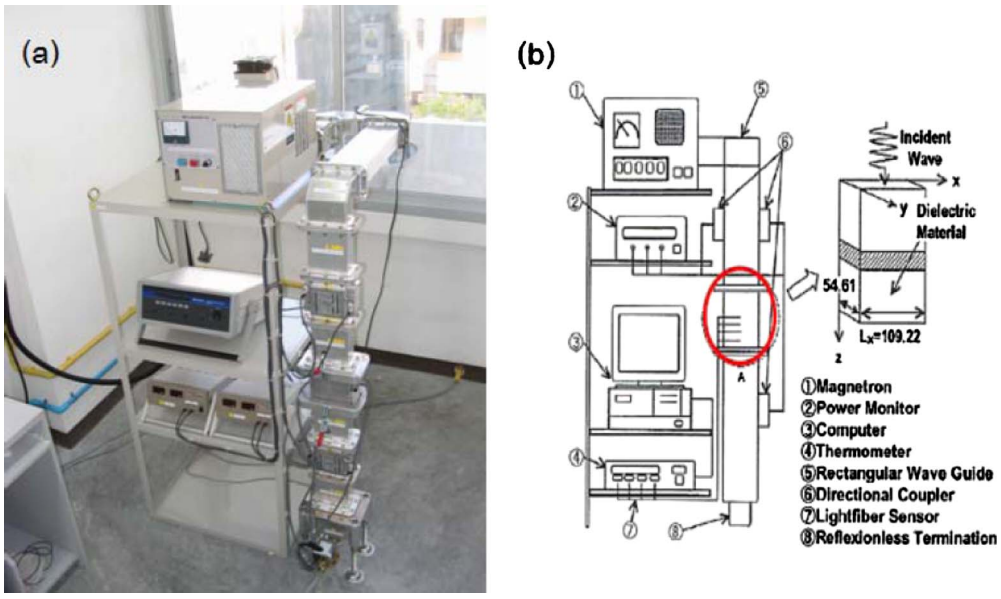

Fig. 1 The microwave heating system with a rectangular waveguide

age to the magnetron. The powers of incident, reflected, and transmitted waves are measured by a wattmeter using a directional coupler (No. 6) (Micro Denshi, Saitama, Japan, model DR-5000). Fiberoptic probes (No. 7) (Luxtron Fluroptic thermometer (model 790, accurate to $\pm 0.5°C$)) are employed for temperature measurement. The probes are inserted into the sample and positioned on the *XZ* plane at $Y=25$ mm (see Fig. 2). Due to the symmetry, temperatures are only measured on one side of the plane. The samples are saturated porous packed beds composed of glass beads and water. The container, with a thickness of 0.75 mm, is made of polypropylene, which does not absorb microwave energy.

In our present experiment, a glass bead of 0.15 mm in diameter is examined. The averaged (freestream) porosity of the packed bed corresponds to 0.385. The dielectric and thermal properties of water, air, and glass bead are listed in Table 1.

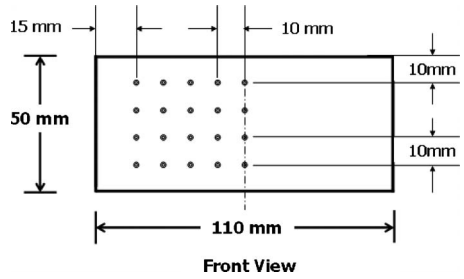

Fig. 2 Locations of temperature measurement in the symmetrical *xz* plane

3 Mathematical Formulation

3.1 Analysis of Electromagnetic Field. Electromagnetic waves are formed with a combination of electric waves and magnetic waves. The magnetic and electric fields of an electromagnetic wave are perpendicular to each other and to the direction of the wave. Microwave is a part of an electromagnetic spectrum that has a particular range of wavelengths. Since the electromagnetic field that is investigated is the microwave field in the TE_{10} mode, there is no variation of field in the direction between the broad faces of the rectangular waveguide and it is uniform in the *y*-direction. Consequently, it is assumed that a two-dimensional heat transfer model in *x*- and *z*-directions will be sufficient to identify the microwave heating phenomena in a rectangular waveguide [7]. Further assumptions are as follows.

(1) The absorption of microwaves by air in a rectangular waveguide is negligible.
(2) The walls of a rectangular waveguide are perfect conductors.
(3) The effect of the sample container on the electromagnetic and temperature fields can be neglected.

The proposed model is considered in the TE_{10} mode so the Maxwell's equations can be written in terms of the electric and magnetic intensities:

$$\varepsilon \frac{\partial E_y}{\partial t} = \frac{\partial H_x}{\partial z} - \frac{\partial H_z}{\partial x} - \sigma E_y \tag{1}$$

Table 1 The electromagnetic and thermophysical properties used in the computations [24]

Property	Water	Glass bead
Heat capacity c_p (J kg^{-1} K^{-1})	4190	800
Thermal conductivity λ (W m^{-1} K^{-1})	0.609	1.0
Density ρ (kg m^{-3})	1000	2500
Dielectric constant,[a] ε_r'	$88.15-0.414T+(0.131\times10^{-2})T^2-(0.046\times10^{-4})T^3$	5.1
Loss tangent,[a] $\tan\delta$	$0.323-(9.499\times10^{-3})T+(1.27\times10^{-4})T^2-(6.13\times10^{-7})T^3$	0.01

[a]T is in °C.

$$\mu\frac{\partial H_z}{\partial t} = -\frac{\partial E_y}{\partial x} \tag{2}$$

$$\mu\frac{\partial H_x}{\partial t} = \frac{\partial E_y}{\partial z} \tag{3}$$

where E and H denote electric field intensity and magnetic field intensity, respectively. Subscripts x, y, and z represent the x-, y-, and z-components of vectors, respectively. Finally, ε is the electrical permittivity, σ is the electrical conductivity, and μ is the magnetic permeability. These variables can be defined as follows:

$$\varepsilon = \varepsilon_0\varepsilon_r \tag{4}$$

$$\mu = \mu_0\mu_r \tag{5}$$

$$\sigma = 2\pi f\varepsilon \tan\delta \tag{6}$$

The dielectric properties of porous material depend on the temperature in which fractions of fluid and solid are considered based on porosity ϕ as follows [23]:

$$\varepsilon_r(T) = \varepsilon_r'(T) - j\varepsilon_r''(T) \tag{7}$$

where

$$\varepsilon_r'(T) = \phi\varepsilon_{rf}'(T) + (1-\phi)\varepsilon_{rp}' \tag{8}$$

$$\varepsilon_r''(T) = \phi\varepsilon_{rf}''(T) + (1-\phi)\varepsilon_{rp}'' \tag{9}$$

where ε' and ε'' represent the dielectric constant and the dielectric loss, respectively.

The loss tangent coefficient can be written as

$$\tan\delta(T) = \frac{\varepsilon_r''(T)}{\varepsilon_r'(T)} \tag{10}$$

When the material is heated unilaterally, it is found that as the dielectric constant and loss tangent coefficient vary, the penetration depth and the electric field within the dielectric material vary. Penetration depth is a measure of how deep the electromagnetic radiation can penetrate into a material. A number of factors can influence penetration depth including properties of the material, intensity, and frequency of the electromagnetic wave. The penetration depth is used to denote the depth at which the power density has decreased to 37% of its initial value at the surface [6].

$$D_p = \frac{1}{\frac{2\pi f}{\upsilon}\sqrt{\frac{\varepsilon_r'\left(\sqrt{1+\left(\frac{\varepsilon_r''}{\varepsilon_r'}\right)^2}-1\right)}{2}}} = \frac{1}{\frac{2\pi f}{\upsilon}\sqrt{\frac{\varepsilon_r'(\sqrt{1+(\tan\delta)^2}-1)}{2}}} \tag{11}$$

where D_p is the penetration depth, ε_r'' is the relative dielectric loss factor, and υ is the microwave speed. The penetration depth of the microwave power is calculated according to Eq. (11), which demonstrates how it depends on the dielectric properties of the material. It is noted that products of huge dimensions and with high loss factors may occasionally overheat a considerably thick layer of the outer surface. To prevent such a phenomenon, the power density must be chosen so that enough time is provided for the essential heat transfer between boundary and core. If the thickness of the material is less than the penetration depth, only a fraction of the supplied energy will become absorbed. For example, the dielectric properties of water show that water moderately dissipate electromagnetic energy into heat. This characteristic depends on the temperature. The water layer at low temperature typically shows a slightly greater potential for absorbing microwaves. In other words, an increase in the temperature typically decreases ε_r'', accompanied by a slight increase in D_p.

The boundary conditions for the TE_{10} mode can be formulated as follows.

(1) Perfectly conducting boundary. Boundary conditions on the inner wall surface of waveguide are given by Faraday's law and Gauss's theorem:

$$E_\parallel = 0, \quad H_\perp = 0 \tag{12}$$

where subscripts $\parallel$ and $\perp$ denote the components of tangential and normal directions, respectively.

(2) Continuity boundary condition. Boundary conditions along the interface between sample and air are given by Ampere's law and Gauss's theorem:

$$E_\parallel = E_\parallel', \quad H_\parallel = H_\parallel' \tag{13}$$

(3) The first-order absorbing boundary condition applied at both ends of rectangular waveguide:

$$\frac{\partial E_y}{\partial t} = \pm\upsilon\frac{\partial E_y}{\partial z} \tag{14}$$

where $\pm$ represents forward and backward directions and υ is the velocity of the wave.

(4) The incident wave due to magnetron is given in Ref. [7], showing an oscillation of the electric and magnetic intensities by the magnetron:

$$E_y = E_{y_{\text{in}}}\sin\left(\frac{\pi x}{L_x}\right)\sin(2\pi ft) \tag{15}$$

$$H_x = \frac{E_{y_{\text{in}}}}{Z_H}\sin\left(\frac{\pi x}{L_x}\right)\sin(2\pi ft) \tag{16}$$

where $E_{y_{\text{in}}}$ is the input value of electric field intensity, L_x is the length of the rectangular waveguide in the x-direction, and Z_H is the wave impedance defined as

$$Z_H = \frac{\lambda_g Z_l}{\lambda} = \frac{\lambda_g}{\lambda}\sqrt{\frac{\mu}{\varepsilon}} \tag{17}$$

Here, Z_l is the intrinsic impedance dependent on the properties of the material and λ and λ_g are the wavelengths of microwaves in free space and the rectangular waveguide, respectively.

The power flux associated with a propagating electromagnetic wave is expressed by the Poynting vector:

$$s = \frac{1}{2}\text{Re}(E\times H^*) \tag{18}$$

The Poynting theorem allows the evaluation of the microwave power input, which is represented as

$$P_{\text{in}} = \int_A SdA = \frac{A}{4Z_H}E_{y_{\text{in}}}^2 \tag{19}$$

3.2 Analysis of Temperature Profile and Flow Field. The physical problem and coordinate system are depicted in Fig. 3. The microwave is propagating to the xy plane while the transport phenomena on the xz plane are currently investigated. To reduce the complexity of the problem, several assumptions have been offered into the flow and energy equations.

(1) Corresponding to the electromagnetic field, the flow and temperature fields can be assumed to be a two-dimensional plane.
(2) The effect of the phase change is neglected.
(3) Boussinesq approximation is used to account for the effect of the density variation on the buoyancy force.

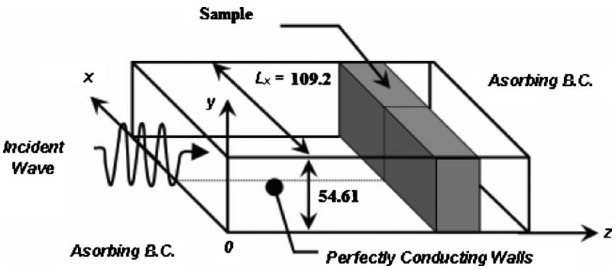

Fig. 3 Schematic of the physical problem

(4) The surroundings of the porous packed bed are insulated except at the upper surface where energy exchanges with the ambient air.

3.2.1 Flow Field Equation. The porous medium is assumed to be homogeneous and thermally isotropic. The saturated fluid within the medium is in a local thermodynamic equilibrium (LTE) with the solid matrix [25–27]. The validity regime of local thermal equilibrium assumption has been established [28]. The fluid flow is unsteady, laminar, and incompressible. The pressure work and viscous dissipation are all assumed to be negligible. The thermophysical properties of the porous medium are taken to be constant; however, the Boussinesq approximation takes into account the effect of density variation on the buoyancy force. The Darcy–Forchheimer–Brinkman model was used to represent the fluid transport within the porous medium [28,29]. The Brinkman's and the Forchheimer's extensions treat the viscous stresses at the bounding walls and the nonlinear drag effect due to the solid matrix, respectively [29]. Furthermore, the solid matrix is made up of spherical particles, while the porosity and permeability of the medium are varied depending on the distance from the wall. Using standard symbols, the governing equations describing the heat transfer phenomenon are given as follows.

Continuity equation:

$$\frac{\partial u}{\partial x}+\frac{\partial w}{\partial z}=0 \tag{20}$$

Momentum equations:

$$\frac{1}{\varepsilon}\frac{\partial u}{\partial t}+\frac{u}{\varepsilon^2}\frac{\partial u}{\partial x}+\frac{w}{\varepsilon^2}\frac{\partial u}{\partial z}=-\frac{1}{\rho_f}\frac{\partial p}{\partial x}+\frac{\nu}{\varepsilon}\left(\frac{\partial^2 u}{\partial x^2}+\frac{\partial^2 u}{\partial z^2}\right)-\frac{\mu u}{\rho_f \kappa}-F(u^2+w^2)^{1/2} \tag{21}$$

$$\frac{1}{\varepsilon}\frac{\partial w}{\partial t}+\frac{u}{\varepsilon^2}\frac{\partial w}{\partial x}+\frac{w}{\varepsilon^2}\frac{\partial w}{\partial z}=-\frac{1}{\rho_f}\frac{\partial p}{\partial z}+\frac{\nu}{\varepsilon}\left(\frac{\partial^2 w}{\partial x^2}+\frac{\partial^2 w}{\partial z^2}\right)-\frac{w\mu}{\rho_f \kappa}-F(u^2+w^2)^{1/2}+g\beta(T-T_0) \tag{22}$$

where ε, ν, and β are the porosity, kinematics viscosity, and coefficient of thermal expansion of the water layer, respectively. The permeability κ and geometric F function are [16,30]

$$\kappa=\frac{d_p^2\varepsilon^3}{175(1-\varepsilon)^2} \tag{23}$$

$$F=\frac{1.75(1-\varepsilon)}{d_p\varepsilon^3} \tag{24}$$

The porosity is assumed to vary exponentially with the distance from the wall [13,15,21]. Based on these previous studies, we proposed the variation of porosity within three confined walls of the bed: a bottom wall and two lateral walls. The expression that considers the variation of porosity in two directions in the xz plane is given by

$$\varepsilon=\varepsilon_s\left[1+b\left\{\exp\left(-\frac{bx}{d_p}\right)+\exp\left(-\frac{b(W-x)}{d_p}\right)+\exp\left(-\frac{bz}{d_p}\right)\right\}\right] \tag{25}$$

where d_p is the diameter of glass beads, ε_s known as the freestream porosity is the porosity far away from the walls, W is the width of the packed bed, and b and c are empirical constants. The dependencies of b and c to the ratio of the bed to bead diameter are small, and b and c were suggested to be 0.98 and 1.0, respectively [14].

3.2.2 Heat Transfer Equation. The temperature of the liquid layer exposed to the incident wave is obtained by solving the conventional heat transport equation with the microwave power absorbed included as a local electromagnetic heat generation term:

$$\sigma\frac{\partial T}{\partial t}+u\frac{\partial T}{\partial x}+w\frac{\partial T}{\partial z}=\alpha\left(\frac{\partial^2 T}{\partial x^2}+\frac{\partial^2 T}{\partial z^2}\right)+Q \tag{26}$$

where the specific heat ratio $\sigma=[\varepsilon(\rho c_p)_f+(1-\varepsilon)(\rho c_p)_s]/(\rho c_p)_f$ and $\alpha=k_e/(\rho c_p)_f$ is the thermal diffusivity.

The local electromagnetic heat generation term that is a function of the electric field is defined as

$$Q=2\pi f\varepsilon_0\varepsilon_r'\tan\delta(E_y)^2 \tag{27}$$

Boundary and initial conditions for these equations. Since the walls of the container are rigid, the velocities are zero. At the interface between the liquid layer and the walls of the container, zero slip boundary conditions are used for the momentum equations.

(1) At the upper surface, the velocity in the normal direction (w) and the shear stress in the horizontal direction are assumed to be zero, where the influence of Marangoni flow [7] can be applied:

$$\eta\frac{\partial u}{\partial z}=-\frac{d\xi}{dT}\frac{\partial T}{\partial x} \tag{28}$$

(2) The walls, except for the top wall, are insulated so no heat or mass exchanges:

$$\frac{\partial T}{\partial x}=\frac{\partial T}{\partial z}=0 \tag{29}$$

(3) Heat is lost from the surface via natural convection and radiation:

$$-\lambda\frac{\partial T}{\partial z}=h_c(T-T_\infty)+\sigma_{\mathrm{rad}}\varepsilon_{\mathrm{rad}}(T^4-T_\infty^4) \tag{30}$$

(4) The initial condition of a medium is defined as

$$T=T_0 \quad \text{at} \quad t=0 \tag{31}$$

4 Numerical Procedure

The description of heat transport and flow pattern of liquid layer equations (20)–(24) and (26) requires specification of temperature (T), velocity components (u,w), and pressure (p). These equations are coupled to the Maxwell's equations (Eqs. (1)–(3)) by Eq. (27), which represents the heating effect of the microwaves in the liquid-container domain.

4.1 Electromagnetic Equations and FDTD Discretization. The electromagnetic equations are solved by using the finite difference time domain (FDTD) method. With this method, the electric field components (E) are stored halfway between the basic nodes while the magnetic field components (H) are stored at the center. Thus, they are calculated at alternating half-time steps. E and H field components are discretized by a central difference method (second-order accurate) in both spatial and time domains.

4.2 Fluid Flow and Heat Transport Equations and Finite Control Volume Discretization. Equations (20)–(24) are solved numerically by using the finite control volume along with the semi-implicit method for pressure-linked equations (SIMPLE) algorithm developed by Patankar. The reason for using this method is the advantage provided by the flux conservation that avoids the generation of a parasitic source. The basic strategy of the finite control volume discretization method is to divide the calculated domain into a number of control volumes and then integrate the conservation equations over this control volume and over an interval of time $[t, t+\Delta t]$. At the boundaries of the calculated domain, the conservation equations are discretized by integrating over half the control volume, taking into account the boundary conditions. At the corners of the calculated domain, we used a quarter of the control volume. The fully Euler implicit time discretization finite difference scheme is used to arrive at the solution in time. Additionally, the details about numerical discretization of this method can be found in the recent literature.

4.2.1 The Stability and Accuracy of Calculation. The choice of spatial and temporal resolutions is motivated by reasons of stability and accuracy. To ensure stability of the time stepping algorithm, Δt must be chosen to satisfy the Courant stability condition and is defined as

$$\Delta t \leq \frac{\sqrt{(\Delta x)^2 + (\Delta z)^2}}{v} \tag{32}$$

and the spatial resolution of each cell is defined as

$$\Delta x, \Delta z \leq \frac{\lambda_g}{10\sqrt{\varepsilon_r}} \tag{33}$$

Corresponding to Eqs. (32) and (33), the calculation conditions are as follows.

(1) Grid resolution is $100(x) \times 200(z)$.
(2) Grid size: $\Delta x = 1.0922$ mm and $\Delta z = 1.0000$ mm.
(3) Time steps: $\Delta t = 2 \times 10^{-12}$ s and $\Delta t = 0.01$ s are used corresponding to the electromagnetic field and temperature field calculations, respectively.
(4) Relative error in the iteration procedures of 10^{-6} was chosen.

The mesh of 100×200 was found to be sufficient for the simulations carried out in the present study. Independence of the solutions on the grid size was examined through a number of test cases. The results indicate that negligible difference of solutions was achieved above the resolution of 80×160 [7].

4.2.2 The Iterative Computational Schemes. Since the dielectric properties of liquid layer samples are temperature dependent, to understand the influence of the electromagnetic fields on the microwave heating of a liquid layer, it is necessary to consider the coupling between electric field and temperature and fluid flow fields. For this reason, iterative computational schemes are required to resolve the coupled nonlinear Maxwell's equations, momentum, and heat transport equations.

The computational scheme is to first compute a local heat generation term by running an electromagnetic calculation with uniform properties determined from initial temperature data. The electromagnetic calculation is performed until a sufficient period is reached in which the representative average root mean square (rms) of the electric field at each point is computed and used to solve the time dependent temperature and velocity field. Using these temperatures, new values of the dielectric properties are calculated and used to recalculate the electromagnetic fields and then the microwave power absorption. All the steps are repeated until the required heating time is reached.

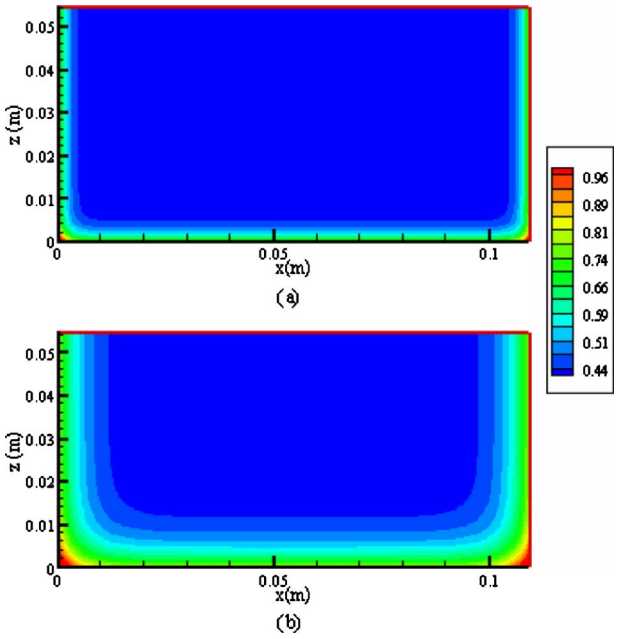

Fig. 4 Porosity distributions with the bead diameters: (*a*) 1 mm and (*b*) 3 mm

5 Results and Discussion

In the current simulations, the formulation that computes the variation of porosity in two directions given by Eq. (25) is employed to describe the two-dimensional porosity variation. The glass bead diameters of 1.0 mm and 3.0 mm are examined with which the freestream porosity is 0.385. The resulting calculations are illustrated in Fig. 4 on the x-z plane. Variations of the bed porosity were considered since it was proved that the porosity decayed from the wall [13,14]. As is clearly seen in the figure, the porosity is high in the vicinity of an impermeable boundary and reduces to a freestream value at about four to five bead diameters from the boundary [15]. The computed porosities vary according to the distances from the walls in two directions. Porosities are largest at the corners because it is not efficient to pack spherical beads at bed corners. The gradients of porosity are found to be lower with larger particle diameters.

To examine the validity of the mathematical model, the numerical results were compared with the experimental data. The description with regard to the experimental setup and associated

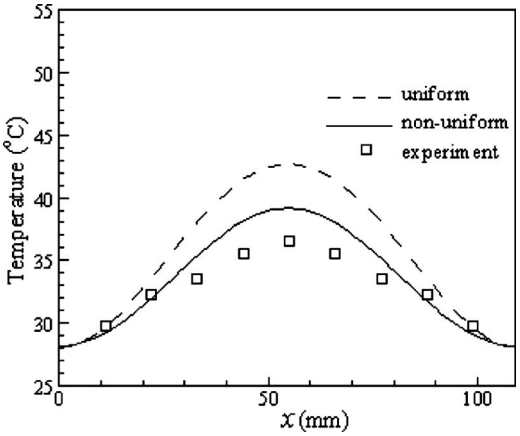

Fig. 5 The temperature distributions taken at 30 s are shown to compare the numerical solutions with the experimental result

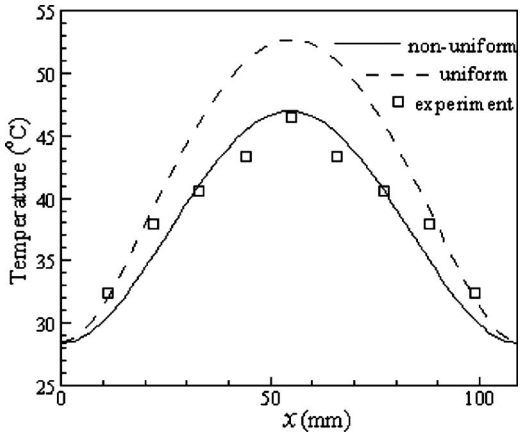

Fig. 6 The temperature distributions taken at 50 s are shown to compare the numerical solutions with the experimental result

parameters is given in Sec. 2. The diameter of glass beads and the freestream porosity are 0.15 mm and 0.385, respectively. With respect to the model simulation, the computed data for both uniform and nonuniform (variable) cases were extracted at 30 s and 50 s. The comparisons of temperature distributions on the x-z plane at the horizontal line $z=21$ mm are shown in Figs. 5 and 6 at 30 s and 50 s, respectively. The results show an appreciably improved agreement when the variation of porosity within the packed bed is considered. For the uniform case, the peak temperature is about 40°C at 30 s and reaches 50°C at a later time, while the temperatures are lower in the case of variable porosity. However, it is clear in both the figures that the temperature is highest at the middle location since the density of the electric field in the TE_{10} mode is high around the center region in the waveguide.

Figure 7 displays temperature contours as a function of time of the two cases, which exhibit a wavy behavior corresponding to the resonance of electric field. For the nonuniform porosity, the heating rate is noticeably slower than that for the uniform porosity. The reason behind this is that in the nonuniform-porosity medium, greater water content exists near the bottom wall attributed to a higher water-filled pore density. Since water is very lossy, large amounts of energy can be absorbed as both the incoming waves and the reflected waves particularly attenuate at the bottom area. This occurrence results in a resonance of a weaker standing wave with smaller amplitude throughout the packed bed. The weaker standing wave dissipates less energy, which is in turn converted into less thermal energy, giving a relatively slow heating rate. This explains why nonuniform porosity gives an overall lower temperature. Furthermore, a greater amount of water present in the

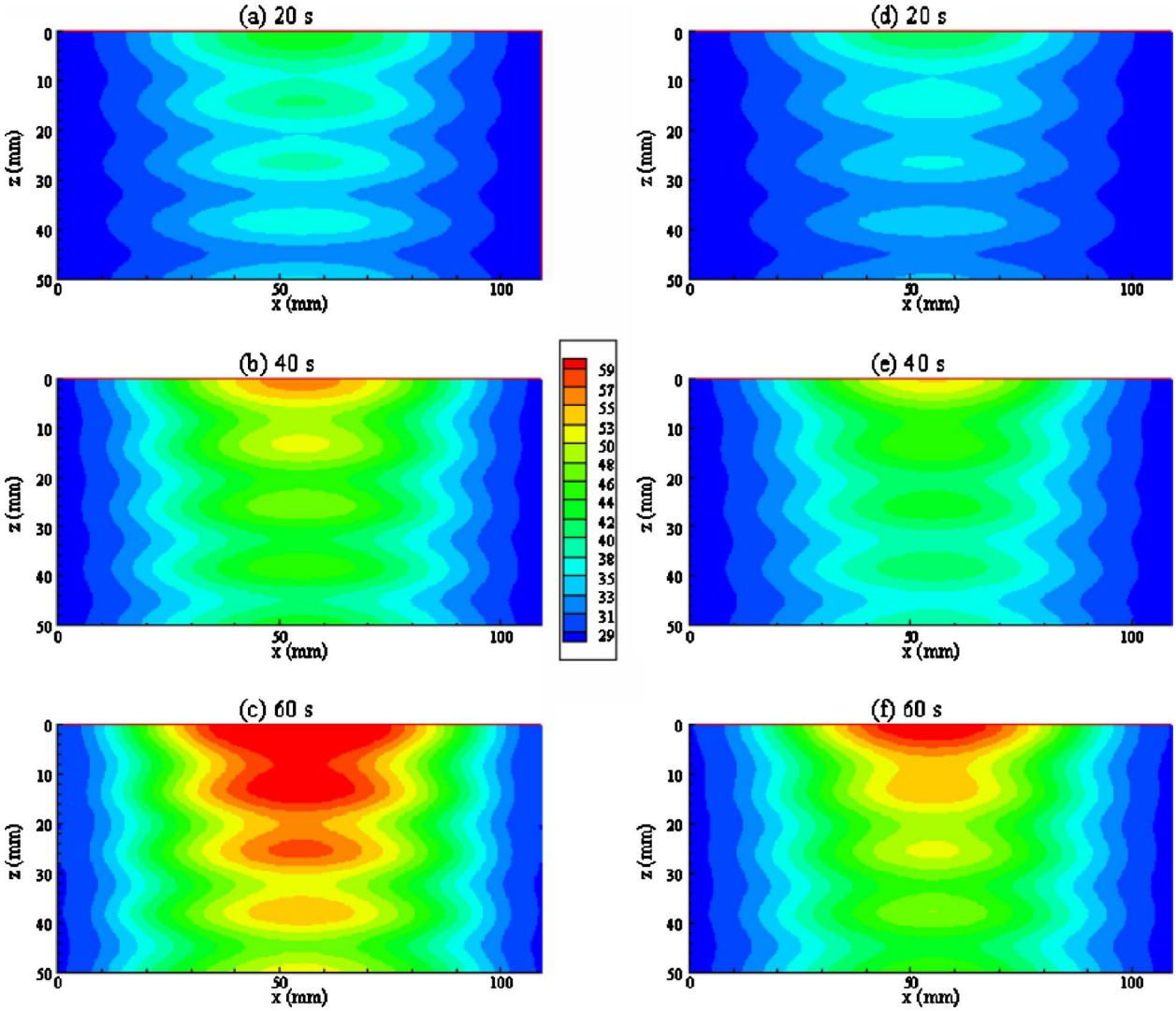

Fig. 7 Time evolutions of temperature contour (°C) within the porous bed at 20 s, 40 s, and 60 s for uniform case ((*a*)–(*c*)) and nonuniform case ((*d*)–(*f*))

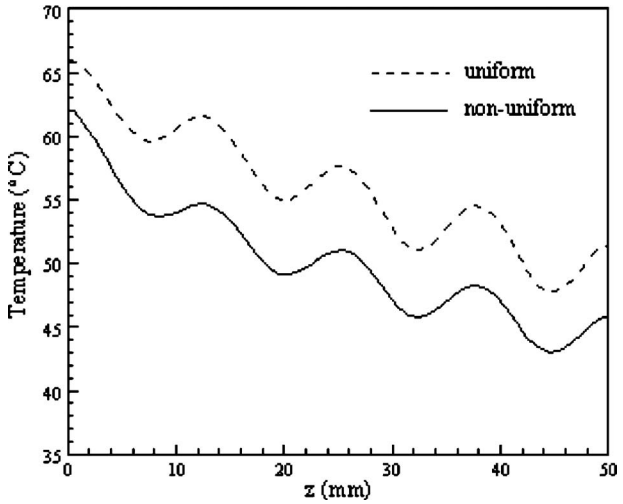

Fig. 8 Centerline temperature along the *z* axis for uniform (dashed line) and nonuniform (solid line) porous packed beds

nonuniform medium causes a smaller depth of penetration since water has relatively high values of dielectric constant and a high loss tangent. Figure 8 shows variations of centerline temperature vertically along the z axis at the different times of the two bed types. The resulting plots confirm the wavy behavior shown in Fig. 7. Moreover, it is obvious that the bed temperature is higher in the uniform-porosity porous bed.

In terms of flow characteristic, the instantaneous velocity vectors at 60 s are displayed in Fig. 9. The fluid flows as it is driven by the effect of buoyancy that overcomes the retarding viscous force. The nonuniform temperature distribution evident in Fig. 7 leads to an unstable condition. Temperature gradients, which exist in both transverse and axial directions, result in circulated flows. The velocities are higher close to the top boundary since there exist higher temperature gradients, thereby higher density gradients leading to stronger buoyancy-induced flows. It is seen that flow velocities in the variable-porosity medium are lower than those in the uniform-porosity medium. This result is attributed to higher porosities near walls in the nonuniform case. Higher porosity media correspond to higher permeability, which allows greater flow velocity due to smaller boundary and inertial effects. The difference is clear in the vicinity of walls where high velocities carry energy from the wall toward the inner area.

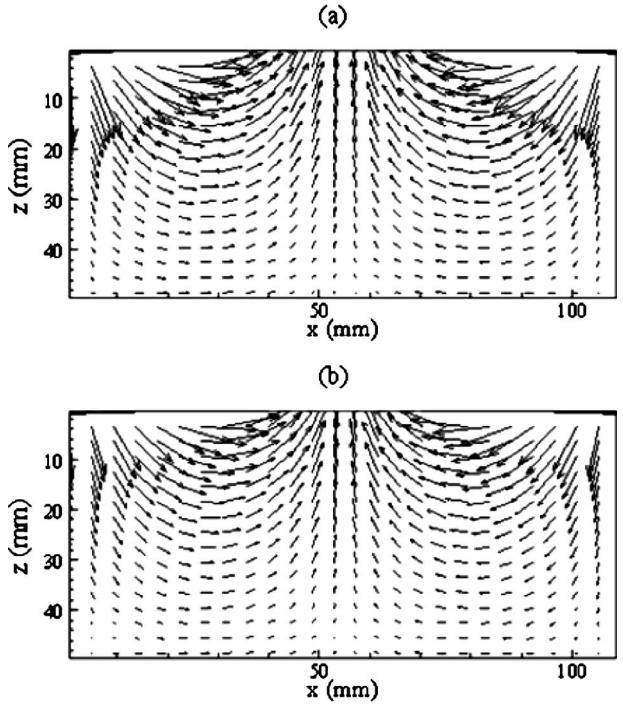

Fig. 9 Velocity vectors from the two cases of porous medium: (*a*) nonuniform and (*b*) uniform

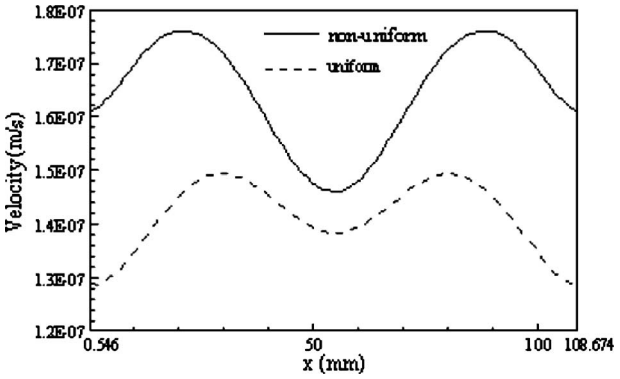

Fig. 10 Variations of velocity magnitudes along the *x* axis for uniform (dashed line) and nonuniform (solid line) porous packed beds

To gain further insight in flow phenomena, the centerline velocity magnitudes along the x-direction are depicted in Fig. 10. It is clear that the nonuniform porosity gives larger magnitudes. Two peaks are seen spatially in both the cases. The peak values are at the same locations, as observed in Fig. 9. More importantly, the gradient of magnitude is larger in the nonuniform case due to the presence of porosity gradients. It is worthwhile comparing a u-component velocity shown in Fig. 11 along the x axis. The sign of the value reflects the direction of flow along the x axis. Relatively cold fluid flows toward the center domain from both sides to replace a hot fluid portion that expands toward the top boundary. This result is consistent with the flow behaviors depicted in Fig. 9.

6 Conclusions

The microwave heating of a porous medium with a nonuniform (variable) porosity is carried out based on the proposed numerical model. The two-dimensional variation of porosity of the medium is considered to be a function of the distance from the bed walls. Transient Maxwell's equations are employed to solve for the description of the electromagnetic field in the waveguide and medium. The generalized non-Darcian model that takes into account

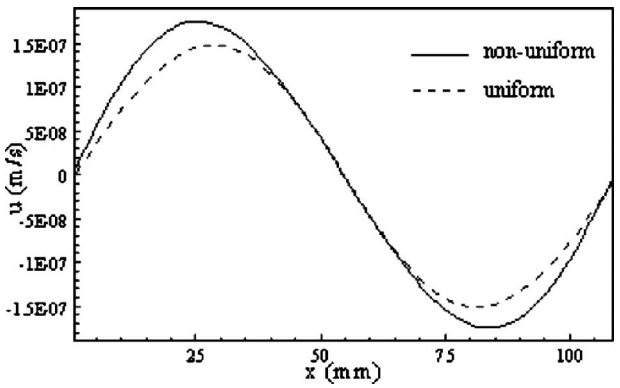

Fig. 11 Variations of *u*-component velocity along the *x* axis for uniform (dashed line) and nonuniform (solid line) porous packed beds

the presence of a solid drag and the inertial effect is included. The numerical results are in good agreement with the experimental data. In addition to the effect on the convective flow velocity that is larger in the nonuniform case, it is found that the variation of porosity near the wall has an important influence on the dielectric properties of the porous packed bed and markedly affects the heating process.

Acknowledgment

This work was supported by the National Research University Project of Thailand Office of Higher Education Commission and by the Thailand Research Fund.

Nomenclature

c_p = specific heat capacity (J/(kg K))
E = electric field intensity (V/m)
f = frequency of incident wave (Hz)
g = gravitational constant (m/s^2)
H = magnetic field intensity (A/m)
P = power (W)
p = pressure (Pa)
Q = local electromagnetic heat generation term (W/m^3)
s = Poynting vector (W/m^2)
T = temperature (°C)
t = time (s)
$\tan \delta$ = dielectric loss coefficient (−)
u,w = velocity component (m/s)
Z_H = wave impedance (Ω)
Z_l = intrinsic impedance (Ω)

Greek Letters

ϕ = porosity (m^3/m^3)
α = thermal diffusivity (m^2/s)
β = coefficient of thermal expansion (1/K)
η = absolute viscosity (Pa s)
ε = permittivity (F/m)
ε' = dielectric constant (F/m)
ε'' = dielectric loss factor (F/m)
λ = wavelength (m)
μ = magnetic permeability (H/m)
υ = velocity of propagation (m/s)
ν = kinematics viscosity (m^2/s)
ρ = density (kg/m^3)
σ = electric conductivity (S/m)
ω = angular frequency (rad/s)
ξ = surface tension (N/m)

Subscripts

0 = free space
∞ = ambient condition
a = air
f = fluid
j = layer number
in = input
p = particle
r = relative

References

[1] Wei, C. K., Davis, H. T., Davis, E. A., and Gordon, J., 1985, "Heat and Mass Transfer in Water-Laden Sandstone: Microwave Heating," AIChE J., **31**(5), pp. 842–848.
[2] Ni, H., Datta, A. K., and Torrance, K. E., 1999, "Moisture Transport in Intensive Microwave Heating of Biomaterials: Porous Media Model," Int. J. Heat Mass Transfer, **42**, pp. 1501–1512.
[3] Feng, H., Tang, J., Cavalieri, R. P., and Plumb, O. A., 2001, "Heat and Mass Transport in Microwave Drying of Porous Materials in a Spouted Bed," AIChE J., **47**, pp. 1499–1512.
[4] Ratanadecho, P., Aoki, K., and Akahori, M., 2002, "Influence of Irradiation Time, Particle Sizes, and Initial Moisture Content During Microwave Drying of Multi-Layered Capillary Porous Materials," ASME J. Heat Transfer, **124**(1), pp. 151–161.
[5] Dinčov, D. D., Parrot, K. A., and Pericleous, K. A., 2004, "Heat and Mass Transfer in Two-Phase Porous Materials Under Intensive Microwave Heating," J. Food Eng., **65**, pp. 403–412.
[6] Rattanadecho, P., 2006, "The Simulation of Microwave Heating of Wood Using a Rectangular Wave Guide: Influence of Frequency and Sample Size," Chem. Eng. Sci., **61**, pp. 4798–4811.
[7] Ratanadecho, P., Aoki, K., and Akahori, M., 2002, "A Numerical and Experimental Investigation of Modelling of Microwave Heating for Liquid Layers Using a Rectangular Wave Guide (Effects of Natural Convection and Dielectric Properties)," Appl. Math. Model., **26**, pp. 449–472.
[8] Cha-um, W., Rattanadecho, P., and Pakdee, W., 2009, "Experimental Analysis of Microwave Heating of Dielectric Materials Using a Rectangular Wave Guide (MODE: TE_{10}) (Case Study: Water Layer and Saturated Porous Medium)," Exp. Therm. Fluid Sci., **33**(3), pp. 472–481.
[9] Ayappa, K. G., and Brandon, S., 1994, "Microwave Driven Convection in a Square Cavity," AIChE J., **40**(7), pp. 1268–1272.
[10] Franca, A. S., and Haghighi, K., 1996, "Adaptive Finite Element Analysis of Microwave Driven Convection," Int. Commun. Heat Mass Transfer, **23**(2), pp. 177–186.
[11] Chatterjee, S., Basak, T., and Das, S. K., 2007, "Microwave Driven Convection in a Rotating Cylindrical Cavity: A Numerical Study," J. Food Eng., **79**, pp. 1269–1279.
[12] Liu, S., and Masliyah, J. H., 1996, "Single Fluid Flow in Porous Media," Chem. Eng. Commun., **148**, pp. 653–732.
[13] Benenati, R. F., and Brosilow, C. B., 1962, "Void Fraction Distribution in Pack Beds," AIChE J., **8**, pp. 359–361.
[14] Vafai, K., 1984, "Convective Flow and Heat Transfer in Variable-Porosity Media," J. Fluid Mech., **147**, pp. 233–259.
[15] Amiri, A., and Vafai, K., 1994, "Analysis of Dispersion Effects and Non-Thermal Equilibrium, Non-Darcian, Variable Porosity Incompressible Flow Through Porous Media," Int. J. Heat Mass Transfer, **37**(6), pp. 939–954.
[16] Khaled, A.-R. A., and Chamkha, A. J., 2001, "Variable Porosity and Thermal Dispersion Effects on Coupled Heat and Mass Transfer by Natural Convection From a Surface Embedded in a Non-Metallic Porous Medium," Int. J. Numer. Methods Heat Fluid Flow, **11**(5), pp. 413–429.
[17] Hsiao, S.-W., Cheng, P., and Chen, C.-K., 1992, "Non-Uniform Porosity and Thermal Dispersion Effects on Natural Convection About a Heated Horizontal Cylinder in an Enclosed Porous Medium," Int. J. Heat Mass Transfer, **35**(12), pp. 3407–3418.
[18] Sakamoto, H., and Kulacki, F. A., 2008, "Effective Thermal Diffusivity of Porous Media in the Wall Vicinity," ASME J. Heat Transfer, **130**(2), p. 022601.
[19] Vafai, K., 1986, "Analysis of the Channeling Effect in Variable Porosity Media," ASME J. Energy Resour. Technol., **108**, pp. 131–139.
[20] Hunt, M. L., and Tien, C. L., 1998, "Non-Darcian Convection in Cylindrical Packed Beds," ASME J. Heat Transfer, **110**, pp. 2523–2532.
[21] Poulikakos, D., and Renken, K., 1987, "Forced Convection in a Channel Filled With Porous Medium, Including the Effects of Flow Inertia, Variable Porosity and Brinkman Friction," ASME J. Heat Transfer, **109**, pp. 880–888.
[22] Chai, Z., and Guo, Z., 2007, "Study of Electro-Osmotic Flows in Microchannels Packed With Variable Porosity Media via Lattice Boltzmann Method," J. Appl. Phys., **101**, p. 104913.
[23] Akbal, S., and Baytas, F., 2008, "Effects of Non-Uniform Porosity on Double Diffusive Natural Convection in a Porous Cavity With Partially Permeable Wall," Int. J. Therm. Sci., **47**(7), pp. 875–885.
[24] Ratanadecho, P., Aoki, K., and Akahori, M., 2001, "Experimental and Numerical Study of Microwave Drying in Unsaturated Porous Material," Int. Commun. Heat Mass Transfer, **28**(5), pp. 605–616.
[25] El-Refaee, M. M., Elsayed, M. M., Al-Najem, N. M., and Noor, A. A., 1998, "Natural Convection in Partially Cooled Tilted Cavities," Int. J. Numer. Methods Fluids, **28**, pp. 477–499.
[26] Nield, D. A., and Bejan, A., 1999, *Convection in Porous Media*, Springer, New York.
[27] Al-Amiri, A. A., 2002, "Natural Convection in Porous Enclosures: The Application of the Two-Energy Equation Model," Numer. Heat Transfer, Part A, **41**, pp. 817–834.
[28] Marafie, A., and Vafai, K., 2001, "Analysis of Non-Darcian Effects on Temperature Differentials in Porous Media," Int. J. Heat Mass Transfer, **44**, pp. 4401–4411.
[29] Nithiarasu, P., Seetharamu, K. N., and Sundararajan, T., 1997, "Natural Convective Heat Transfer in a Fluid Saturated Variable Porosity Medium," Int. J. Heat Mass Transfer, **40**, pp. 3955–3967.
[30] Chamkha, A. J., Issa, C., and Khanafer, K., 2002, "Natural Convection From an Inclined Plate Embedded in a Variable Porosity Porous Medium Due to Solar Radiation," Int. J. Therm. Sci., **41**, pp. 73–81.